2011 American Control Conference
on O'Farrell Street, San Francisco, CA, USA
June 29 - July 01, 2011

Nitrogen blanketing front equilibria in dead end anode fuel cell operation

Jixin Chen, Jason B. Siegel, and Anna G. Stefanopoulou

Abstract— **This paper investigates the equilibrium behavior during the dead-ended anode (DEA) operation of a proton exchange membrane fuel cell. A reduced order model is developed focusing on the species molar fraction in the anode channel. At equilibrium, hydrogen is present only in a partial region in the anode, and the remaining region is deactivated by the accumulation of water and nitrogen. Simulation results are analysed to study the influences of certain controllable inputs and system parameters on the nitrogen front location and steady-state cell voltage. The simulation results are consistent with the initial experimental observations. The results in this paper suggest that it is possible to coat only the active portion of the membrane, along the channel length, with catalyst.**

I. Introduction

Dead-end anode (DEA) operation was previously proposed and implemented by several groups [1], [2], [3], because such operation greatly simplifies the system by removing the inlet humidification and hydrogen recirculation hardware. During DEA operation, the nitrogen and liquid water accumulate in the anode channel and are pushed to the outlet, causing a gradual drop in cell voltage over time. Purges are thus necessary to remove nitrogen/water from the anode and to recover the voltage.

The objective of this work is to explore the equilibrium in DEA operation and study the key operating parameters controlling the equilibrium and fuel cell terminal voltage. Simulations of dynamic models [4], [5] have shown such equilibria. The local catalyst loading could be applied non-uniformly, based on the local hydrogen distribution in steady state, so that the catalyst could be utilized much more efficiently in PEM fuel cells with DEAs.

Our prior work [4] includes a dynamic model capturing the species concentrations, membrane water content, local current density along the channel and cell voltage. The model predicted anode nitrogen blanketing and liquid water plugging as unique features of DEA operation and shows that N_2 blanketing is the most significant mechanism and the primary cause of the gradual, yet recoverable voltage drop. The dynamic model has been verified by in-situ gas chromatography measurement and neutron imaging [4]. The local difference between anode and cathode species partial pressure drive transport through membrane with a rate constant that depends on the membrane water content. Although the gas phase crossover proceeds at a fairly low rate due to the low permeability of membrane, the accumulation effects over time have an integrator type behavior. Therefore periodic purging of the accumulated inert gas is required for high power operation. The generally repeatable patterns of cell voltage and species concentration between purges simplify the water management by reducing the randomness of water behavior in the fuel cell [6], [7]. The co-flow and vertical orientation of the fuel cell channels result in the nitrogen/water accumulation at the bottom of the anode channel with the front moving towards the inlet.

Funding is provided by the National Science Foundation. The authors are with the Fuel Cell Control Laboratory, University Michigan, Ann Arbor, MI 48109, USA. Email: jixinc@umich.edu (J. Chen)

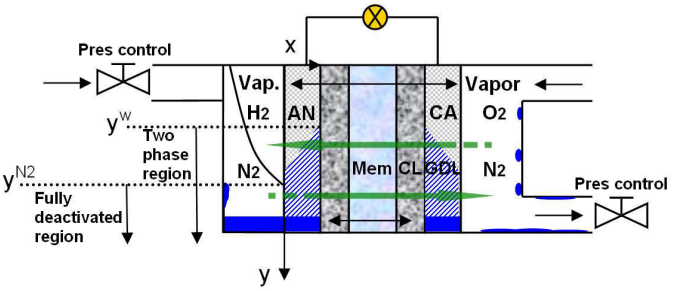

Fig. 1. Equilibrium scenario in DEA operation (not to scale). The net flux of nitrogen and water is from anode to cathode in the channel end region, as opposed to other regions.

II. Equilibrium Mechanism

The concept of equilibrium for nitrogen accumulation based on a single volume lumped parameter model is easy to visualize as shown in Fig. 1. In the simplest form, when the purge valve is closed, no nitrogen can enter or leave the system except to cross though the membrane; therefore the nitrogen accumulation is governed by the following ordinary differential equation (ODE)

$$\frac{\mathrm{d}P_{N_2,an}}{\mathrm{d}t} = K_{N_2}\frac{A_{fc}}{RTV_{an}\Delta_{mb}}(P_{N_2,ca} - P_{N_2,an}) \quad (1)$$

where A_{fc} is the membrane area, V_{an} is the anode volume and Δ_{mb} is the membrane thickness, and K_{N_2} is the nitrogen permeation rate though the membrane. The accumulation continues until the averaged partial pressure of N_2 in the anode channel is equal to that of air in the cathode volume (assuming uniform membrane water content, and hence uniform K_{N_2}, along the length of the channel). In [5] and [8] we show the effects of convection pushing and packing the nitrogen at the bottom of the channel and preventing hydrogen from reaching that portion of the channel. In this case the local nitrogen partial pressure may easily exceed the cathode, however if the nitrogen permeation rate is constant along the y-direction, the average nitrogen partial pressure on the anode will not exceed the cathode's average, (for small pressure differentials between the anode and cathode volume). Therefore, convection driven dynamics also predict

that dynamically stable equilibrium (with positive cell terminal voltage) exist at low current density, where the active area of the fuel cell is reduced by an amount equal to the mole fraction of nitrogen in the cathode channel (the effective area is reduced by 60 to 80%). In steady state, the nitrogen crossover is from cathode to anode at the upper portion of the channel (negative x-direction), and from anode to cathode in the lower region (positive x-direction), as shown with the arrows of N_2 flux through membrane. In Eq. (2), the inclusion of diffusive terms moderates the effect of nitrogen in the anode channel, by slowing the rate of formation of the nitrogen blanketing region, which is driven by convection. Alternatively stated, the same averaged molar fraction of nitrogen in the anode channel will blanket a smaller region of the fuel cell active area if diffusive effects are included in the model. We establish the existence of equilibrium and their feasibility with respect to a reasonable power producing device, i.e. can the equilibrium result in an acceptable voltage output.

In literature, Benziger and co-works [9], [10], [11] reported the experimentally observed equilibrium in their stirred-tank-reactor (STR) fuel cells using dead-end anode and low humidification (RH 0.3-0.5) for both fuel and air. They identified multiple equilibria of the system using inlet RH as a parameter and focused on the water content variation in the through-membrane (or x-direction). In this paper, a Partial Differential Equation (PDE) based model is used to study the extreme spatial variations of water and nitrogen along the anode (y-direction) and to describe the equilibrium.

III. Along the Channel Model

The major assumptions in the present model [4] are: 1) the catalyst layer is treated as an interface; 2) isothermal both in x and y directions; 3) the oxygen crossover is neglected since it may be completely and quickly reduced at the anode catalyst layer [12]; 4) in-plane current re-distribution is neglected (due to large membrane aspect ratio) [13] and therefore the local current density of H_2 reaction is equal to the cathode oxidization. The 1-D modeling domain (along the y-direction) includes the anode channel, membrane and cathode channel.

The model inputs are the nominal current I, cathode inlet relative humidity (RH), and cathode Stoichiometric Ratio (SR). Temperature T and Anode(AN)/Cathode(CA) inlet pressures P_{ca} / P_{an}, are fixed parameters in the model but may be adjusted prior to simulation, to capture the experimental conditions. The model output is cell voltage, which is physically measurable. The nitrogen blanketing front location $y^{\mathrm{N_2}}$ and the two-phase water front location $y^{\mathrm{H_2O}}$ along the anode channel length are also calculated as they represent important performance metrics. We define $y^{\mathrm{N_2}}$ as the location along the anode channel at which the local hydrogen concentration drops below a critical value, halting the local reaction. The two phase front location, $y^{\mathrm{H_2O}}$, is defined similarly as the point at which the vapor pressure reaches saturation.

A brief discussion of the dynamic states follows. The state variables of interest are the anode channel partial pressures of nitrogen and water vapor, and the membrane water content λ. The Stefan-Maxwell model describes convection, diffusion, and reactions in the anode gas channel,

$$\frac{P_{an}}{RT}\frac{\partial x_i}{\partial t} = -\frac{\partial}{\partial y}\left(J_i + x_i N_t\right) + r_i, \tag{2}$$

for $i = [1,2] = [N_2, H_2O]$, where N_t is the total convective gas flux, J_i is the diffusive flux, and r_i denotes the reaction terms. Only two of the three components are independent in this modeling framework. We chose to model the mole fractions of nitrogen, x_{N_2}, and water vapor, x_{H_2O}, as our dynamics states. Because the mole fractions must sum to one,

$$\sum x_i = 1, \tag{3}$$

we can calculate the hydrogen from the other gases $x_{H_2}(y) = 1 - x_{N_2}(y) - x_{H_2O}(y)$. Note that $x_{H_2O(v)} = \min(x_2, P_{sat}(T)/P_{an,in})$ is used for all the following calculations, including J_i. The remaining water is assumed to be liquid water and is tracked separately; i.e. we are assuming instant condensation.

The boundary condition of Eq. (2) at the inlet is zero concentrations of nitrogen and vapor given fully dry and pure hydrogen supply, and zero diffusive flux of each species:

$$x_i\big|_{y=0} = 0 \tag{4}$$

for $i = [1,2] = [N_2, H_2O]$ and

$$J_i\big|_{y=0} = 0 \tag{5}$$

for $i = [1,2,3] = [N_2, H_2O, H_2]$.

At the outlet, the convective flux is zero except during the purge event:

$$N_t\big|_{y=L} = 0 \ or \ N_{out} \tag{6}$$

In this work $N_{out} = N_{purge}$, a constant. The diffusive flux of each species is also zero at the outlet:

$$J_i\big|_{y=L} = 0 \tag{7}$$

for $i = [1,2,3] = [N_2, H_2O, H_2]$.

The third and final dynamic state in our model is membrane water content, λ, which is governed by diffusion, and electro-osmotic drag.

$$\frac{\partial \lambda}{\partial t} = \frac{\partial}{\partial x} D_w \frac{\partial \lambda}{\partial x}. \tag{8}$$

where D_w is the diffusion coefficient for water in the membrane and the Electro-Osmotic drag term enters the model through the boundary conditions. Due to the use of a very thin membrane, the concentration gradient in the membrane can be approximated by quadratic relationship and the membrane water content distribution represented by a single ODE [14], at each y.

The convective flux, N_t, is driven by the consumption of hydrogen. In Eq. (2), a constant pressure is used as an approximation because the anode volume is fed via pressure

regulation and the straight channel geometry introduces minimal pressure drop along the length of the channel. Although a pressure gradient, corresponding to the convective flux, develops along the length of the channel, the pressure drop is less than 1 Pa at 1 A cm^{-2}, so a constant pressure is valid for calculating the concentrations. The ideal gas law, $PV = nRT$ or $P = cRT$, is used to relate pressure and mole fraction of gas species in the channel.

A causal formulation for the diffusive fluxes is used [21]

$$\begin{bmatrix} J_1 \\ J_2 \end{bmatrix} = -\frac{P_{an}}{RT\phi(x)} \begin{bmatrix} D_1(x_1), & D_2(x_1) \\ D_3(x_2), & D_4(x_2) \end{bmatrix} \begin{bmatrix} \frac{\partial x_1}{\partial y} \\ \frac{\partial x_2}{\partial y} \end{bmatrix}, \tag{9}$$

where

$$\begin{aligned} D_1(x_1) &= (1-x_1)D_{13}D_{12} + x_1 D_{23}D_{13}\ , \\ D_2(x_1) &= -x_1(D_{23}D_{12} - D_{23}D_{13})\ , \\ D_3(x_2) &= -x_2(D_{13}D_{12} - D_{23}D_{13})\ , \\ D_4(x_2) &= (1-x_2)D_{23}D_{12} + x_2 D_{23}D_{13}\ , \end{aligned} \tag{10}$$

and D_{ij} are the temperature-dependent binary diffusion coefficients from Ref. [15]. $\phi(x)$ is given by

$$\phi(x) = (D_{23} - D_{12})x_1 + (D_{13} - D_{12})x_2. \tag{11}$$

Conservation of mass allows solving of Eq. (2) for $N_t(y)$, assuming the outlet flow is known $N_t(L) = N_{out}$. The equation for conservation of mass can be written as,

$$\frac{\partial N_t}{\partial y} = \sum r_i, \tag{12}$$

because $\sum J_i = 0$ by definition. Then the convective flux along the channel can be found from Eq. (12) by integrating backward in space along the channel,

$$\begin{aligned} N_t(y) = N_t(L) + \int_y^L (&n_{H_2,rct}(\tilde{y}) + n_{N_2,crs}(\tilde{y}) \\ &+ n_{H_2O,crs}(\tilde{y}))\mathrm{d}\tilde{y}. \end{aligned} \tag{13}$$

anode is purging.

The source term for nitrogen in the AN CH is membrane crossover, which is calculated from the difference in nitrogen partial pressure across the membrane of thickness Δ_{mb},

$$\begin{aligned} n_{N_2,crs}(y) = &-K_{N_2}(T,\lambda_{mb})(w_{an,ch} + w_{an,rib}) \\ &\times \frac{(P_{N_2,ca,mb}(y) - P_{N_2,an,mb}(y))}{\Delta_{mb}}. \end{aligned} \tag{14}$$

We assume that the permeation takes place both over the ribs and channels $(w_{an,ch} + w_{an,rib})$, where w_* indicates the width of each. The partial pressure of nitrogen at each membrane surface is calculated using the following expressions, $P_{N_2,an,mb}(y) = x_{N_2}(y)\ P_{an,in}$ and $P_{N_2,ca,mb}(y) = P_{ca,in} - P_{v,ca}(y) - P_{O_2,ca,mb}(y)$, assuming uniform pressure everywhere. The oxygen/vapor concentration at the cathode, $P_{O_2,ca,mb}(y)/P_{v,ca}(y)$, is calculated using local current density $i_{fc}(y)$ (see [4]). The nitrogen permeation rate $K_{N_2}(T,\lambda_{mb})$ (see [4]) depends both on temperature and membrane water content.

The hydrogen reaction rate is calculated from the local current density,

$$n_{H_2,rct}(y) = \frac{i_{fc}(y)}{2F}(w_{an,ch} + w_{an,rib}), \tag{15}$$

where F is Faraday's constant.

The source term for water vapor in the anode channel is also membrane crossover, which is calculated from the diffusion and electro-osmotic drag

$$n_{H_2O,crs} = \left(\frac{\lambda^*_{an} - \lambda^*_{ca}}{R_{w,mb}} + n_d\frac{i_{fc}(y)}{F}\right)(w_{an,ch} + w_{an,rib}) \tag{16}$$

where λ^* is the equilibrium value of membrane water content, a function of RH in the channel. $R_{w,mb}$ is the resistance to membrane transport [4] and n_d is the coefficient of electro-osmotic drag. λ^* is related to the vapor partial pressure in the anode:

$$\lambda^* = 0.043 + 17.81RH - 39.85RH^2 + 36RH^3 \tag{17}$$

$$RH = x_{H_2O}(y)\frac{P_{an,in}}{P_{sat}(T)} \tag{18}$$

where P_{sat} is the saturation pressure.

Table I lists the parameter values used in the simulation. The simulation results are discussed in the next section.

TABLE I

GEOMETRICAL, PHYSICAL AND OPERATING PARAMETERS

Quantity	**Value**
Active MEA area A_{fc}	50 cm^2
Channel depth h_{ca}/h_{an}	0.1/0.18 cm
Channel width $w_{ca,ch}/w_{an,ch}$	0.069/0.208 cm
Channel length L_{ch}	7.27 cm
Rib width $w_{ca,rib}/w_{an,rib}$	0.076/0.084 cm
Membrane thickness δ_{mb}	20μm
Stack temperature T_{st}	70°C
Transfer coefficient for hydrogen reaction α_{H_2}	0.5
Transfer coefficient for oxygen reaction α_{O_2}	0.5
Exchange current density of hydrogen reaction i_{0,H_2}	$0.5 \times 10^{-2} A/cm^2$
Exchange current density of oxygen reaction i_{0,O_2}	$0.7 \times 10^{-9} A/cm^2$
Charge concentration in membrane c_f	$1.2 \times 10^3 mol/m^3$

IV. RESULTS AND DISCUSSION

A. Model validation

Before presenting the simulation results, preliminary experiments are performed with a 50 cm^2 effective area single cell to validate the calculated equilibria. In Fig. 2 the results from experiments and simulations are co-plotted. The time is zero-referenced from each anode purge, and plotted for three subsequent purge cycles. The current density is increased after the first purge from 0.2 to 0.3 A cm^{-2}. The voltage responses verify the expected equilibria as discussed in Section II. In the case of 0.3 A cm^{-2}, the model predicted equilibrium voltage is very close the experimental result. The erratic voltage behavior after achieving equilibrium can

be attributed to the random formulation and transport of water droplets in the cathode channel. The discrepancy of equilibrium voltage in the case of 0.2 A cm^{-2} may be due to the cathode channel flooding, which leads to the overestimate of the model.

B. Influences of cathode pressure

Fig. 3 shows the simulation results obtained under different cathode pressure levels for P_{AN}=1.05P_{CA}. The simulation model inputs are i=0.2 A cm^{-2} and cathode RH/SR=0.6/2. A distinct trend observed in Fig. 3 is that

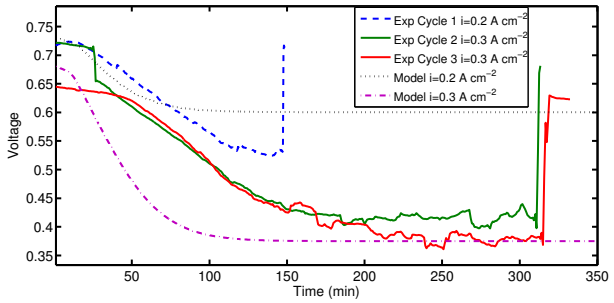

Fig. 2. Experimental results showing time evolution and convergence to voltage equilibrium for two different current set-points (P_{CA}=1.58 bar, T_{st}=65°C, cathode RH/λ=0.6/2.5, i_{ave}=0.2, 0.3 A cm^{-2})

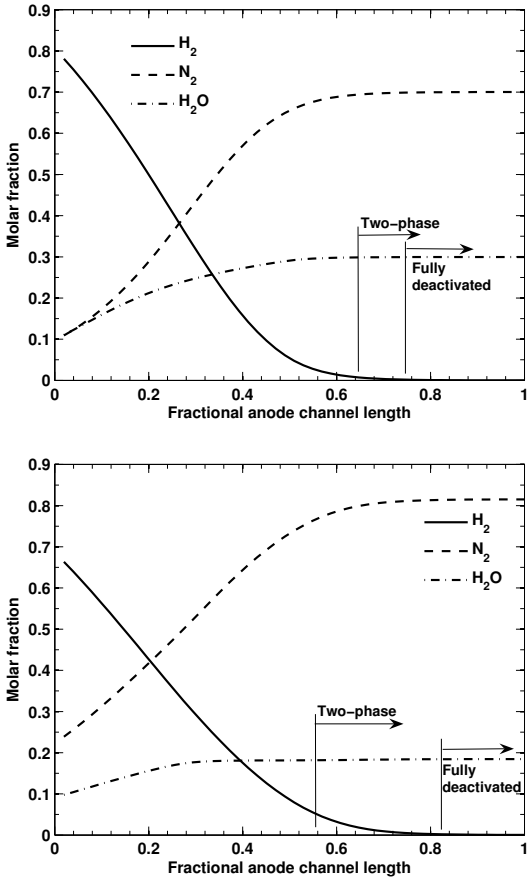

Fig. 3. Species molar fractions at equilibrium with different system pressures (top P_{CA}=1.18 bar and bottom P_{CA}=1.58 bar)

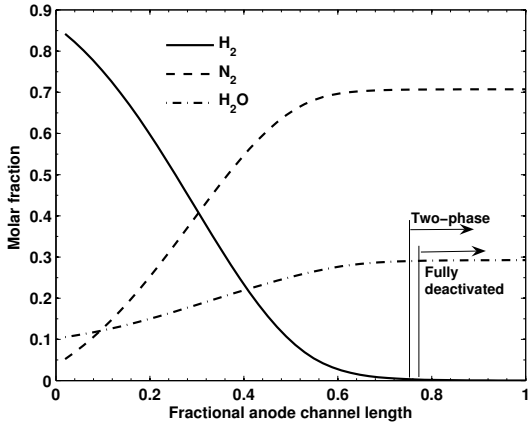

Fig. 4. Species molar fractions at equilibrium with low RH ($i_{ave} = 0.2A\ cm^{-2}$, $\text{RH}_{CA,in} = 0.1$,$P_{CA} = 1.18bar$)

increasing system pressure moves the nitrogen blanketing front towards the channel end. The fully deactivated area is only ~17% of the channel if the pressure can be maintained at ~1.6 bar. The channel two phase front moves with a reverse trend towards the channel inlet, mainly because of the additional water entering the cathode channel as pressure increases. Furthermore, Fig. 5 shows that increasing pressure results in more uniform local current distribution, as the blanketing effects are reduced.

Although beneficial, the increased system pressure in DEA operation has other system-level issues, particularly the anode sealing may be more likely to fail under higher pressure. Hydrogen itself can readily diffuse into the sealing material and gradually damage its original structure. In addition, simply increasing pressure for better outputs may not be economic overall due to the cost of pressurization in a real system and the efficiency loss [22].

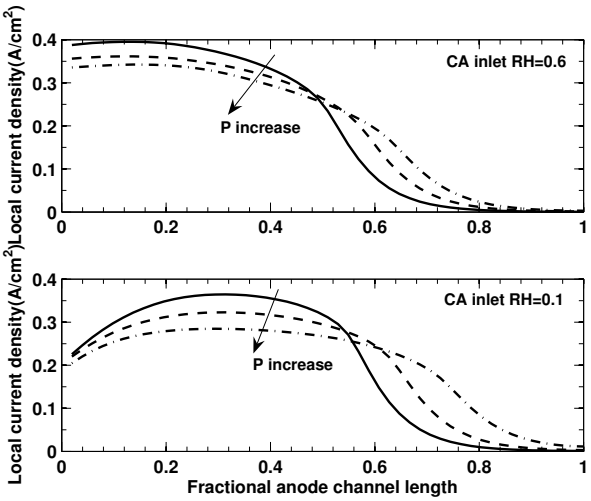

Fig. 5. Local current densities at equilibrium with different pressures (P_{CA}=1.18, 1.38, 1.58 bar, RH=0.6, 0.1, $i_{ave} = 0.2A\ cm^{-2}$)

C. Influences of cathode inlet RH

The influences from cathode inlet RH can be observed by comparing Fig. 4 and top subplot of Fig. 3. As expected, the low RH pushes the two phase front towards the end. In the case of $\mathrm{RH}_{CA,in} = 0.1$, the channel two phase front is very close to the fully blanketing front. It should be noted that the RH variation gives small influence on the anode distribution of species concentration at equilibrium. From the local current profile (Fig. 5), it is shown that for RH=0.1, the current density distribution exhibits non-monotonic behavior due to the dry inlet conditions, and the gradual self-humidification achieved towards the mid-channel region. The simulation suggests that if the low RH can be combined with high pressure, the blanketing may be alleviated and the local current distribution is more uniform among all cases considered.

D. Influences of cathode stoichiometry

The cathode stoichiometry plays very limited role in determining the cell voltage within the range of 2-3 (normal selection for PEM fuel cell operation). With decreasing cathode stoichiometry, the consumption of oxygen would increase the partial pressure of nitrogen significantly.

E. Evolution towards equilibrium

The time evolutions of the molar fractions along the channel are shown in Fig. 6 and Fig. 7 The molar fractions at 10%, 50% and 98% of the channel length are selected to represent the conditions of the entrance, middle and end regions of the anode channel. The simulation results show that the voltage evolution follows the trend of the hydrogen concentration at mid-channel region. Note that the cell voltage equilibrates after the species concentrations of the whole channel have stabilized, thus the molar fractions at the end region actually reach the steady state much earlier than the system equilibrium due to the slow propagation of the front. The evolution profiles shown in Fig. 7 indicate that the change of molar fractions reach steady state at ~3000s.

Table II presents four important parameters at equilibrium, obtained at different average current density and RH but the same pressure and temperature. The time constant for cell voltage τ_V is defined as the time from 10% to 90% of the full voltage step. $P_{N_2}^{eq}$ is the channel-averaged nitrogen partial pressure at equilibrium, and y^{N_2} the nitrogen blanketing front as indicated in Fig. 1.

From the simulation, high current reduces the equilibrium voltage, resulting in longer time to reach the equilibrium voltage. At higher RH (0.6), there would be more water in the MEA and channel and hence larger time constant. However, increasing RH from 0.1 to 0.6 may only give very small performance improvement (~$0.01V$) at equilibrium, thus the stable equilibrium output (if achievable) may be more dependent on the system pressure rather than the RH of supply, supporting the idea of a self-humidified high utilization fuel cell. The N_2 partial pressure reduces with increasing current because of the associated higher vapor pressure at the cathode. Finally, elevated current moves the complete blanketing front towards the inlet. Based on the equilibrium front location, we can change the local catalyst loading. The fully deactivated region may need very little catalyst coating. Modeling work such as this paper is the first step in designing such novel fuel cell.

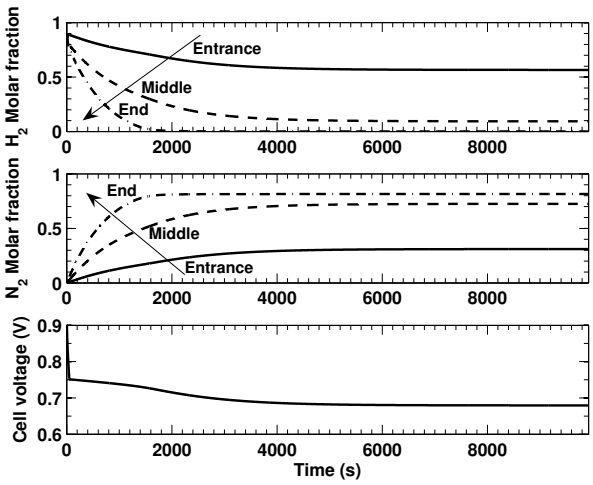

Fig. 6. Cell voltage and species molar fractions approaching the equilibrium ($P_{CA} = 1.58$ bar, RH/$\lambda = 0.6/2, i_{ave} = 0.2A\ cm^{-2}$)

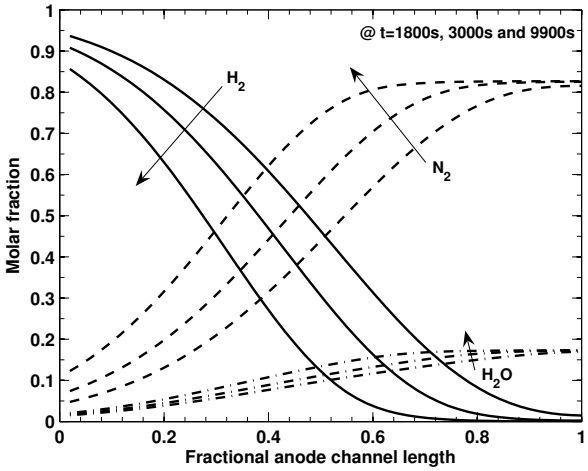

Fig. 7. Dynamic evolution of species molar fractions, shown selected times at 1800s, 3000s and 9900s, ($P_{CA} = 1.58$ bar, RH/$\lambda = 0.6/2, i_{ave} = 0.2A\ cm^{-2}$)

F. Implications to fuel cell design and operation

The simulation results indicate that in DEA operation, if equilibrium could be maintained, the performance is satisfactory at low RH and relatively low pressure, which are achieved with partial electrode region fully deactivated. Therefore, the fuel cell may be manufactured with the MEA non-catalyzed in that deactivated region if the model predicted y^{N_2} can be validated with experiments. Also, the catalyst loading may be adjusted based on the uneven local hydrogen distribution in the simulation.

TABLE II

SELECTED PARAMETER VALUES AT EQUILIBRIUM WITH T_{st}=70°C AND $P_{CA} = 1.58bar$

RH=0.1 i_{ave} A/cm^2	V_{cell}^{eq} V	y^{N_2}	$P_{N_2}^{eq}$, bar	i_{max} A/cm^2	τ_V s
0.1	0.78	0.80	1.10	0.123	3944
0.2	0.68	0.75	1.06	0.285	4304
0.3	0.57	0.67	1.05	0.500	4935
0.4	0.45	0.63	1.03	0.761	5858
RH=0.6 i_{ave} A/cm^2	V_{cell}^{eq} V	y^{N_2}	$P_{N_2}^{eq}$ bar	i_{max} A/cm^2	τ_V s
0.1	0.79	0.86	1.08	0.159	4150
0.2	0.69	0.75	1.06	0.342	4746
0.3	0.57	0.63	1.04	0.599	5023
0.4	0.45	0.59	1.03	0.902	6089

The benefits of DEA operation are the high utilization of anode fuel, and reduced requirement of humidification. The elevated system pressure is also beneficial. Future work is needed to evaluate the attraction to the stability for these equilibria and the transition between equilibrium. Note that at high current, the cell may shutdown quickly even before the membrane becomes well humidified, and that is why we selected $0.2A\ cm^{-2}$ in parametric studies. There are very few experimental observation in literature which reported the steady state outputs of PEM fuel cell with DEA, the only one found being [1]. Also, the present model has not included the H_2/O_2 crossover effects, which may produce additional decay in steady state outputs, as well as safety concerns.

V. CONCLUSIONS

In this work, we used our 1D along-channel, isothermal and dynamic model [4] to study the equilibrium in PEM fuel cell DEA operations. The DEA fuel cell cannot support high power density but could target low-cost/portable applications. The anode species concentration, channel two phase front and fully deactivated front due to nitrogen blanketing and water flooding in anode were examined under different operating conditions. Cell voltage is less dependent on the cathode RH compared with pressure. Cathode (system) pressure may influence the voltage output at equilibrium more significantly, not only affecting the kinetic but also moving the fully blanketing and two phase fronts. Current drawn from the cell may be the most important parameter which determines the blanketing front and the time constant for reaching system equilibrium. The large variation of local current density suggested that spatially-varying catalyst loading based on local hydrogen profile in equilibrium may be preferred. The model predicted equilibria have been validated against the preliminary experimental results. Future work includes additional experiments to validate the equilibrium under extended current loads and the stability of equilibrium.

REFERENCES

[1] P. Mocoteguy, F. Druart, Y. Bultel, S. Besse, and A. Rakotondrainibe, "Monodimensional modeling and experimental study of the dynamic behavior of proton exchange membrane fuel cell stack operating in dead-end mode," *Journal of Power Sources*, vol. 167, pp. 349–357, 2007.

[2] D. McKay, J. Siegel, W. Ott, and A. Stefanopoulou, "Parameterization and prediction of temporal fuel cell voltage behavior during flooding and drying conditions," *Journal of Power Sources*, vol. 178, pp. 207–222, 2008.

[3] J. Siegel, D. McKay, A. Stefanopoulou, D. Hussey, and D. Jacobson, "Measurement of liquid water accumulation in a pemfc with dead-ended anode," *Journal of Electrochemical Society*, vol. 155, pp. B1168–B1178, 2008.

[4] J. Siegel, S. Bohac, A. Stefanopoulou, and S. Yesilyurt, "Nitrogen front evolution in purged polymer electrolyte membrane fuel cell with dead-ended anode," *Journal of Electrochemical Society*, vol. 157, pp. B1081–B1093, 2010.

[5] E. Muller, F. Kolb, L. Guzzella, A. Stefanopoulou, and D. McKay, "Correlating nitrogen accumulation with temporal fuel cell performance," *Journal of Fuel Cell Science and Technology*, vol. 7, pp. 021013–1–021013–11, 2010.

[6] K. Jiao, J. Park and X. Li, "Experimental investigations on liquid water removal from the gas diffusion layer by reactant flow in a PEM fuel cell," *Applied Energy*, vol. 87, pp. 2770–2777, 2010.

[7] J. Chen and B. Zhou, "Diagnosis of PEM fuel cell stack dynamic behaviors," *Journal of Power Sources*, vol. 177, pp. 83–95, 2008.

[8] E. Muller, F. Kolb, A. Stefanopoulou, D. McKay and L. Guzzella, "Correlating nitrogen accumulation with temporal fuel cell performance," *Proc. of Dynamic Systems and Control Conference (DSCC08)*, vol. 7, Paper TuAT5.1, 2008.

[9] J. Benziger, E. Chia, E. Karnas, J. Moxley, C. Teuscher, and I. Kevrekidis, "The stirred tank reactor polymer electrolyte membrane fuel cell," *AIChE Journal*, vol. 50, pp. 1889–1990, 2004.

[10] C. Woo and J. Benziger, "PEM fuel cell current regulation by fuel feed control," *Chemical Engineering Science*, vol. 62, pp. 957–968, 2007.

[11] W. Hogarth and J. Benziger, "Operation of polymer electrolyte membrane fuel cells with dry feeds: Design and operating strategies," *Journal of Power Sources*, vol. 159, pp. 968–978, 2006.

[12] J. Nam, P. Chippar, W. Kim, and H. Ju, "Numerical analysis of gas crossover effects in polymer electrolyte fuel cells (PEFCs)," *Applied Energy*, vol. 87, pp. 3699–3709, 2010.

[13] J. Meyers and R. Darling, "Model of carbon corrosion in PEM fuel cells," *Journal of Electrochemical Society*, vol. 153, pp. A1432–A1442, 2006.

[14] K. Promislow, P. Chang, H. Haas and B. Wetton, "Two-phase unit cell model for slow transients in polymer electrolyte fuel cells," *Journal of Electrochemical Society*, vol. 155, pp. A494–A504, 2008.

[15] T. Berning and N. Djilali, "A 3D, Multiphase, Multicomponent Model of the Cathode and Anode of a PEM Fuel Cell," *Journal of Electrochemical Society*, vol. 150, pp. A1589–A1598, 2003.

[16] R. Ahluwalia and X. Wang, "Buildup of nitrogen in direct hydrogen polymer-electrolyte fuel cell stacks," *Journal of Power Sources*, vol. 171, pp. 63–71, 2007.

[17] K. Jiao and X. Li, "Three-dimensional multiphase modeling of cold start processes in polymer electrolyte membrane fuel cells," *Electrochimica Acta*, vol. 54, pp. 6876–6891, 2009.

[18] P. Berg, K. Promislow, J. S. Pierre, J. Stumper, and B. Wetton, "Water management in pem fuel cells," *Journal of Electrochemical Society*, vol. 151, pp. A341–A353, 2004.

[19] S. Ge, X. Li, B. Yi, and I.-M. Hsing, "Absorption, desorption, and transport of water in polymer electrolyte membrane fuel cells," *Journal of Electrochemical Society*, vol. 152, pp. A1149–A1157, 2005.

[20] I. Hussaini and C.-Y. Wang, "Visualization and quantification of cathode channel flooding in PEM fuel cells," *Journal of Power Sources*, vol. 187, pp. 444–451, 2008.

[21] N. Amundson, T.-W. Pan and V. Paulsen, "Diffusion with Stefan and Maxwell," *AIChE Journal*, vol. 49, pp. 813–830, 2003.

[22] J. Pukrushpan, A. Stefanopoulou and H. Peng, "Control of fuel cell breathing," *IEEE Control Systems Magazine*, vol. 24, pp. 30–46, 2004.